P189   MACHINE LEARNING ALGORITHMS FOR TROPICAL CYCLONE CENTER FIXING AND EYE DETECTION

Robert DeMaria[*]
CIRA/CSU, Fort Collins, CO, USA

Galina Chirokova
CIRA/CSU, Fort Collins, CO, USA

John Knaff
NOAA/NESDIS/StAR, Fort Collins, CO, USA

Jack Dostalek
CIRA/CSU, Fort Collins, CO, USA

1. INTRODUCTION

Formation of a tropical cyclone eye is often associated with the beginning of rapid intensification, so long as the environment remains favorable (Vigh et al, 2012). Thus, determining the onset of eye formation is very important for intensity forecasts. By the same token, eye formation is also important for tropical cyclone location estimation as the cyclone's center becomes obvious when an eye is present.

Currently the determination of eye formation from satellite imagery is generally performed subjectively as part of the Dvorak intensity estimate and/or official warning/advisory/discussion processes. At present, little investigation has been made into the use of objective techniques. As a consequence, much of the satellite imagery available to depict eye-formation is not used. Therefore objective automated methods of performing eye detection are highly desirable 1) to improve tropical cyclone intensity forecasts and 2) to assist automated tropical cyclone center fixing algorithms. This also implies that different center fixing methods likely are needed depending on whether an image contains an eye.

2. EYE DETECTION DATA

A dataset consisting of 2684 IR images contained in the CIRA/RAMMB TC image archive (Knaff et al. 2014) from the years 1989-2013, and comprising just those tropical cyclone cases with maximum wind speed greater than 50 knots (26 ms^{-1}) has been assembled for use with this project. Within each of these images, an area of 80x80 pixels near the storm center, as determined from Automated Tropical Cyclone Forecasts (ATCF; Sampson and Schrader 2000) best track data data, was selected for use with the algorithm. This area was unrolled to form a 6400 element vector. Each vector was inspected for missing data. Seven vectors were excluded due to missing data, leaving 2677 "good" vectors. Finally, all of the "good" vectors were combined to form a 2677x6400 element matrix. Each image has an eye or no-eye classification associated with it which was derived from information contained in the operational Dvorak intensity fixes (see Velden 2006) produced by the Tropical Analysis and Forecast Branch (TAFB) at the National Hurricane Center (NHC). These fixes are typically generated every six hours and are considered truth for the algorithm development described here.
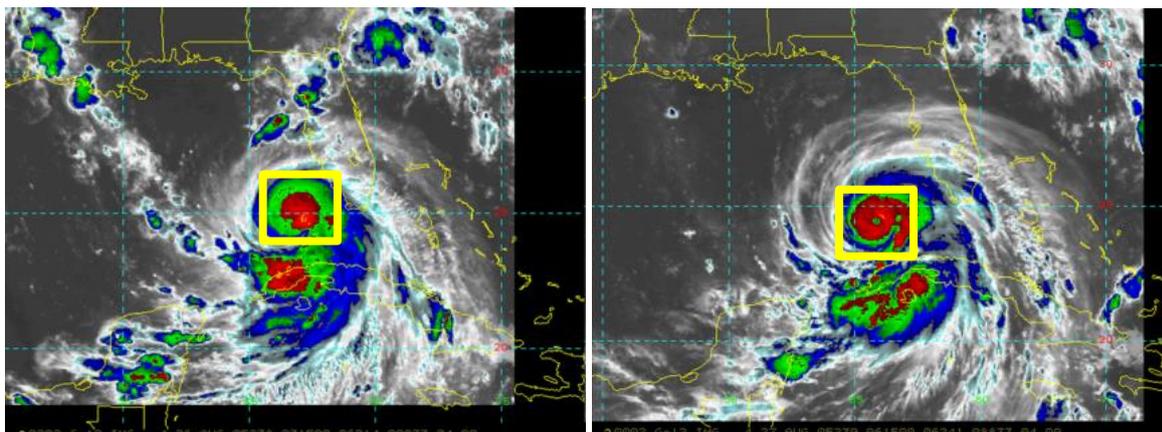

Figure 1. Example IR images from Hurricane Katrina. Boxes show the selection of pixels used with the algorithm. Image classified as "eye absent" (left). Image classified as "eye present" (right)

---

* *Corresponding author address*: Robert DeMaria
CIRA, Colorado State University, 1375 Campus Delivery,
Fort Collins, CO 80523-1375; e-mail: Robert.DeMaria@colostate.edu

Based on that information, IR images were placed into one of the two categories: "Eye Present" or "Eye Absent". Approximately 60% of the data was subjectively classified as "Eye-Absent" and the remaining 40% was classified as "Eye-Present". To evaluate the quality of the eye detection, these data were randomly shuffled and partitioned so 70% of the data would be used for training and 30% would be used for testing. Figure 1 shows consecutive six-hourly images for Hurricane Katrina. In this case, the image on the left was classified as " Eye Absent" and the image on the right was classified as "Eye Present."

3. PRINCIPLE COMPONENT ANALYSIS/CLASS SEPARABILITY

Each raw sample (i.e., image) used in this project is represented by a 6400 element vector. However, only 2677 samples are available for use in this project. This relatively low number of samples compared to the dimensionality of the data does not sufficiently explain the state space

represented by 6400 dimensions. For this reason, dimension reduction using Principle Component Analysis (PCA) (Zito et al, 2008) was performed on the training dataset. As a result, 11 eigenvectors were found that account for 90% of the variance of the data. By projecting the training and testing data onto these eigenvectors, the dimension of the data are reduced: the data were projected from a 2677x6400 element matrix to a 2677x11 element matrix.

This dimension reduction allows for the separability of the two classes to be inspected. To do this, the principle components were first generated for each image. All images with an eye and all those without an eye were then averaged. Figure 2 (a) shows resulting mean principle components for the "Eye-Absent" and "Eye-Present" classes. Several of these principle components show a clear separation between the two classes. Figure 2 (b-d) show eigenvectors 0 (b), 1 (c), and 3 (d) which provide the best separation as seen on Figure 2 (a).
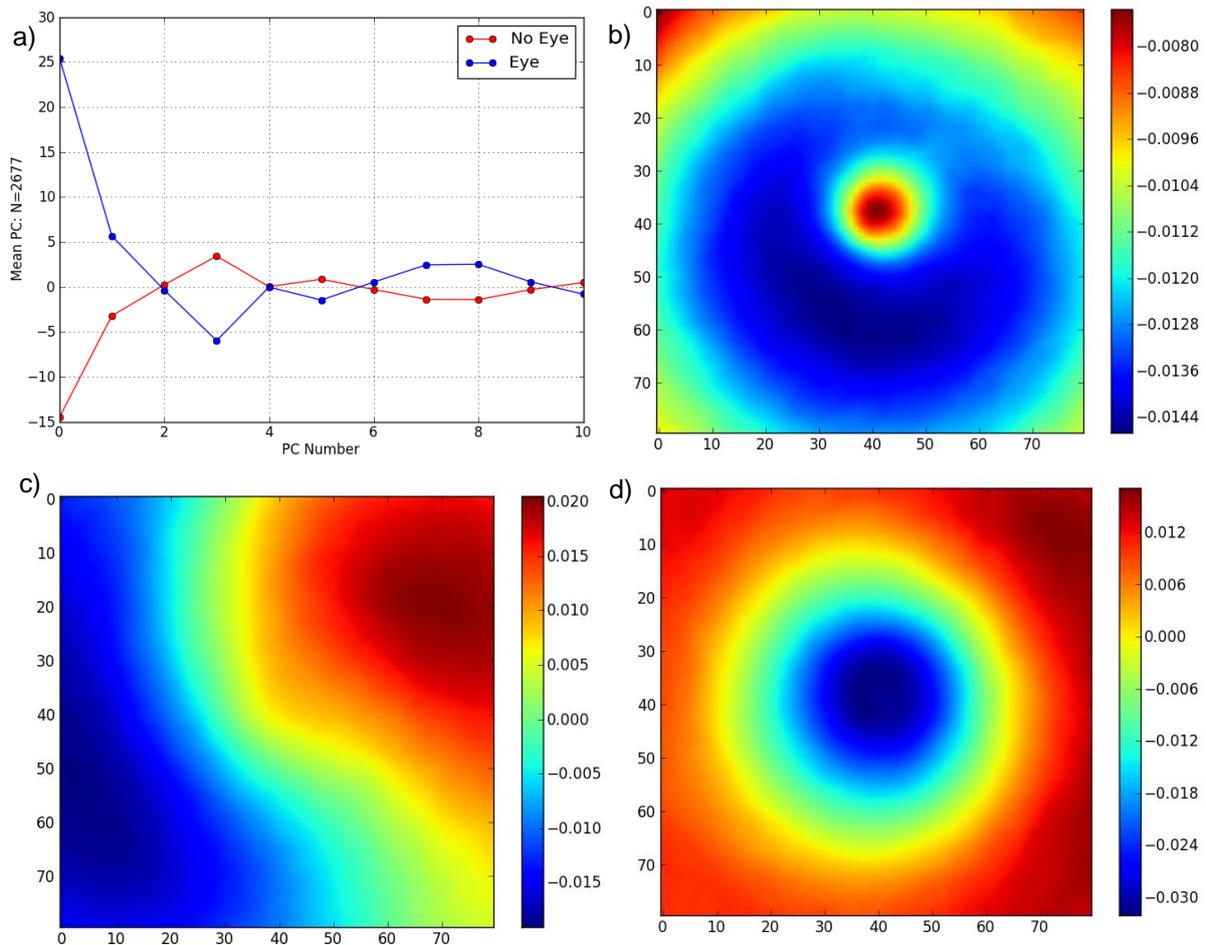

Figure 2. (a) Mean principle components for the "Eye-Absent" and "Eye-Present" classes. Eigenvectors 0, 1 and 3 seem to separate the two classes the best. (b-d) Eigenvectors produced from the IR dataset. Eigenvector 0 (top), eigenvector 1 (left), eigenvector 3 (right).

4. QUADRATIC DISCRIMINANT ANALYSIS

The training set with reduced dimension was used to train a Quadratic Discriminant Analysis (QDA) implementation (Zito et al, 2008). Among the many machine learning algorithms available to perform classification, QDA was selected primarily for its relative simplicity. Additionally, the output of the algorithm can be used to generate a confidence measure for each classification. The schematics of using QDA algorithms for training and classification are shown on Figure 3.

Estimated classifications were then generated for each of the images in the testing set. To perform training, the dimension reduced IR images together with the subjective classification, which are considered to be truth, were used as an input to the QDA. To perform classification, each IR image was used as an input to QDA, and the algorithm produced an estimated classification. These estimated classifications were then compared to the subjective classifications to measure the error. Further work will be performed to produce confidence measures.
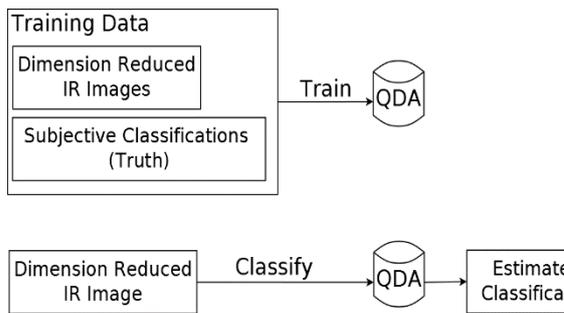
Figure 3: Once trained, the QDA implementation can be used to perform classification on new images not belonging to the training set.
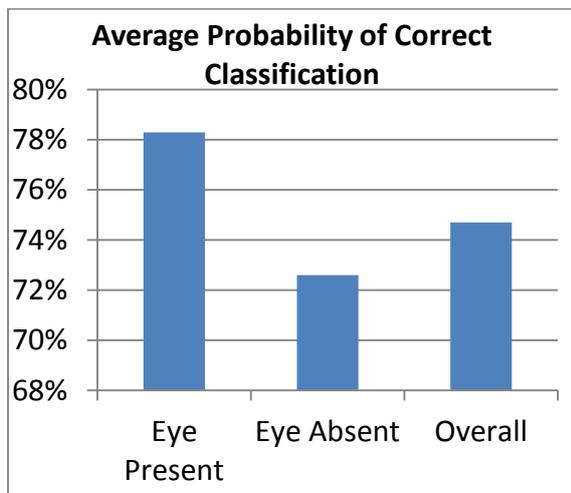
Figure 4. Average probability that an image will be correctly classified.

5. PRELIMINARY RESULTS

In order to gain an accurate view of how well the eye-detection algorithm performs, the estimated classifications obtained with QDA were compared to the previously generated subjective classification performed by the TAFB at NHC. To ensure that the accuracy of the algorithm was not an anomaly bound to a particular shuffling of the original data, the algorithm was run 1200 times. Each time the input data was shuffled and then partitioned into different training and testing sets. Figures 4 and 5 show the accuracy and error statistics averaged over all of these runs. Figure 4 shows that, on average, roughly 75% of the images were correctly classified. Images with eyes in them were correctly classified approximately 78% of the time, and images without eyes were correctly classified about 72% of the time. Figure 5 illustrates that, on average, 28% of the images without eyes were incorrectly classified (False Positive). Additionally, roughly 22% of the images with eyes were incorrectly classified (False Negative).

Figure 5. Average probability that an image will be incorrectly classified.

6. CONCLUSIONS AND FUTURE PLANS

Further work will be performed to determine which cases the algorithm performs poorly on. In addition, different intensity thresholds will be examined as the 50-knot intensity threshold is a relatively low for eye formation in IR imagery as shown in Vigh et al. (2012). Additional data (e.g., vertical wind shear) may also be added to the input and confidence intervals will be added to the output. It is also desirable to create probabilistic estimates of eye formation using similar information.

One primary goal of this work is to add automated classifications and/or probabilities to the input of statistical-dynamical intensity forecasts to determine whether this information improves the accuracy of the forecast. The eye detection estimates may also be used as input to an automated center-fixing routine that is currently under development. Finally, the possibility of improving the results with the use of high-resolution VIIRS imagery will also be investigated.

DISCLAIMER:

The views, opinions, and findings contained in this article are those of the authors and should not be construed as an official National Oceanic and Atmospheric Administration (NOAA) or U.S. Government position, policy, or decision.

REFERENCES

Velden, C., B. Harper, F. Wells, J. L. Beven II, R. M. Zehr, T. Olander, M. Mayfield, C. Guard, M. Lander, R. Edson, L. Avila, A. Burton, M. Turk, A. Kikuchi, A. Christian, P. Caroff, P. McCrone. 2006: The Dvorak Tropical Cyclone Intensity Estimation Technique. *Bull. Amer. Meteor. Soc.*, pp. 1195-1210.

Vigh, J. L., J.A. Knaff, W. H. Schubert "A Climatology of Hurricane Eye Formation", 2012: *Mon. Wea. Rev.*, **140,** pp. 1405-1426

Knaff, J.A., S.P. Longmore, D.A. Molenar, 2014: An Objective Satellite-Based Tropical Cyclone Size Climatology. *J. Climate*, **27**, 455-476.

Sampson, C.R., and A. J. Schrader, 2000: The automated tropical cyclone forecasting system (Version 3.2). *Bull. Amer. Meteor. Soc.*, **81**, 1231-1240

Zito, T., N. Wilbert, L. Wiskott, and P. Berkes, 2009: Modular toolkit for Data Processing (MDP): a Python data processing frame work. *Front. Neuroinform.* **2:8**. doi:10.3389/neuro.11.008.2008.